*Korean J. Chem. Eng.*, 39(8), 2109-2116 (2022)
DOI: 10.1007/s11814-022-1117-0

pISSN: 0256-1115
eISSN: 1975-7220

# Chlorination behavior of $LiCoO_2$

**Min Ku Jeon*,**,† and Sung-Wook Kim***

*Decommissioning Technology Research Division, Korea Atomic Energy Research Institute, 111, Daedeok-daero 989, Yuseong-gu, Daejeon 34057, Korea
**Department of Quantum Energy Chemical Engineering, University of Science and Technology, 217, Gajeong-ro, Yuseong-gu, Daejeon 34113, Korea
(*Received 5 January 2022 • Revised 10 March 2022 • Accepted 17 March 2022*)

**Abstract**−The chlorination behavior of $LiCoO_2$ (LCO) was investigated as a function of the reaction temperature (400-600 °C) and time (1-8 h) under a 190 mL/min Ar+10 mL/min $Cl_2$ flow. Based on the results of a structural analysis, a sequential reaction mechanism was proposed for the chlorination of LCO: $LiCoO_2 \rightarrow$(400-600 °C) $Li_{1-x}CoO_{2-y} \rightarrow$(450-600 °C) $Co_3O_4 \rightarrow$(500-600 °C) $CoCl_2$. It was also found that thermal decomposition of the $Li_{1-x}CoO_{2-y}$ phase to the $LiCoO_2$ and $Co_3O_4$ phases occurs simultaneously in the temperature range of 550-600 °C, resulting in reduced Li removal ratios. A change in the reaction temperature caused significant changes in the reaction product in terms of the constituent phases and their ratios because each reaction step is independently affected by the reaction temperature. In consideration of the highest Li removal ratio (0.86 after 8 h of the chlorination) and potential loss of Co by sublimation of $CoCl_2$ at elevated temperatures, the optimum suggested temperature for the chlorination of LCO is 500 °C.

Keywords: Cathode Material, Li-ion Battery, X-ray diffraction, Chlorination, Recycle

## INTRODUCTION

Numerous efforts are underway to stop global warming, and the transportation sector is facing rapid changes with the help of technical innovations and governmental support. Despite the 16% drop in global car sales, the registration of electric vehicles (EVs) increased by 41% in 2020 [1]. EVs normally use Li-ion batteries (LIBs) for power, which are known to have a lifespan of 8-10 years [2]. Although used LIBs, disassembled from EVs after the lifespan, can also be used in other areas such as energy storage systems, they will eventually need to be recycled in the near future. At this point, LIBs should be managed carefully due to environmental and economic issues because they contain both toxic chemicals and valuable transition metals. Cathode materials are of great interest from an economic standpoint, as they include transition metals such as Ni, Co, Mn, and Al, of which the cost accounts for around half that of the LIB. Accordingly, the recovery ratio of the transition metals is a key parameter that determines the commercial success of the LIB recycling process.

There are various options for recovering transition metals from cathode materials, including pyrometallurgical and hydrometallurgical methods [2-4], which are the most widely accepted techniques at present. The pyrometallurgical method operates within a high temperature range of 1,000-1,500 °C under an oxidizing atmosphere. Transition metals accumulate at the bottom of the reactor as a mixed ingot, while other metals are vaporized or oxidized to float as slag over the transition-metal ingot. This process appears to be relatively simple; however, the loss of Li by evaporation and the required additional processing of the recovered transition-metal ingot for recycling are major drawbacks. The hydrometallurgical method employs acid solutions to dissolve the cathode materials. Each constituent metal is selectively recovered by adding appropriate precipitation agents or by controlling the pH. This method is most widely used currently due to its low energy consumption and ability to recover each transition metal separately. However, the selectivity of transition-metal recovery is limited due to the similar chemical behavior of transition metals, resulting in the need for the subsequent purification of the recovered transition metals. In addition, an acid solution is produced as a secondary waste [2]. There are other options for the recycling or regeneration of cathode materials. Xu et al. [5] introduced a 'targeted healing' technique in which a $LiFePO_4$ (LFP) cathode was regenerated by low-temperature aqueous solution relithiation followed by rapid post-annealing. Yang et al. [6] employed a LiOH-KOH molten salt system with $LiNO_3$ and $O_2$ oxidants to regenerate $LiCoO_2$ (LCO) through a two-step heating process. Qu et al. [7] reported an $NH_4Cl$ roasting technique that involved the use of $NH_4Cl$ as a chlorinating agent to convert LCO into LiCl and $CoCl_2$. The chlorides were dissolved in water and then selectively recovered by adding NaOH to produce the precipitate $Co(OH)_2$.

Recently, a new approach that utilizes $Cl_2$ gas as a reaction agent to recover transition-metal oxides from $Li(Ni,Co,Mn)O_2$ (Ni : Co : Mn=1 : 1 : 1) was introduced [8]. The following reaction equation is the key to the chlorination technique to achieve the selective conversion of Li into LiCl:

$$LiMO_2+1/2\ Cl_2\ (g) \rightarrow LiCl+1/3\ M_3O_4+1/3\ O_2\ (g) \quad (1)$$

Here, M represents the transition metals of Ni, Co, and Mn. Here, LiCl has a high water-solubility of 84.5 g/100 g $H_2O$ at 25 °C [9], which makes it easy to separate LiCl from the insoluble spinel-type $M_3O_4$ phase in a subsequent water-washing step. It was also found

†To whom correspondence should be addressed.
E-mail: minku@kaeri.re.kr

that some of the transition metals are chlorinated and then dissolved during the water-washing step. However, these transition-metal chlorides can be recovered via a $Na_2CO_3$ precipitation step to reach an overall transition-metal recovery ratio of 94.9 wt%. The advantage of the chlorination process is mainly that it achieves a high transition-metal recovery ratio through a simple process.

Although NCM and LFP are current major products, LCO, the first cathode material for LIBs introduced back in 1979 [10,11], still accounts for a significant portion among the various cathode materials produced today [2]. Accordingly, LCO is currently the major cathode material from a waste standpoint as well. In the present study, the chlorination behavior of LCO is investigated as a function of the reaction temperature and time to identify the feasibility of a new chlorination technique for the recycling of LCO.

## EXPERIMENTAL

Chlorination reaction experiments were conducted using a quartz tube reactor (40 mm diameter) equipped with an electrical furnace in the middle to control the reaction temperature. The quartz tube reactor was positioned horizontally and one end of the reactor was connected to a gas feed system. This system is composed of two mass flow controllers (MFCs) that control the flow rates of Ar (Model 3660, Kofloc Co. Ltd., Japan) and $Cl_2$ (Model 5400, Kofloc Co. Ltd., Japan) independently. The other end of the reactor was connected to a gas exhaust system that includes a dry $Cl_2$ scrubber to remove un-reacted $Cl_2$ from the gas stream. In every experimental trial here, 2.00 g of LCO purchased from MSE Supplies (USA) was employed. After the LCO was weighed, it was loaded into an alumina boat and then placed in the middle of the quartz reactor. The electrical furnace began to heat the reactor to a set temperature after air inside the reactor was purged by flowing Ar at a rate of 200 mL/min for at least 2 h. When the reactor reached the set temperature with a ramping rate of 10 °C/min, the flow rates of the MFCs changed to 190 and 10 mL/min for Ar and $Cl_2$, respectively. The chlorination reaction experiments were conducted at 400, 450, 500, 550, and 600 °C for 1, 2, 4, and 8 h at each temperature. The samples prepared in this work are listed in Table 1. Sample names include information about the reaction temperature and time. For example, LCO-500-4 represents the LCO specimen reacted at 500 °C for 4 h under a 190 mL/min Ar+10 mL/min $Cl_2$ flow. The flow rates of Ar and $Cl_2$ are not included in the sample name because all experiments were conducted under an identical flow of 190 mL/min Ar+ 10 mL/min $Cl_2$. When the reaction finished, the $Cl_2$ flow rate was set to zero and the reactor was cooled to room temperature. The LCO samples were immersed in 100 mL of DI (deionized) water for at least 15 h before filtering. The filtered samples were washed using 100 mL of DI water and then dried at 120 °C for 2 h in an oven.

**Table 1. A list of the samples prepared in this study. The gas flow rate was fixed at 190 mL/min Ar+10 mL/min $Cl_2$ in all samples**

| Sample name | Reaction temperature | Reaction time |
|---|---|---|
| LCO-400-1 | 400 °C | 1 h |
| LCO-400-2 | 400 °C | 2 h |
| LCO-400-4 | 400 °C | 4 h |
| LCO-400-8 | 400 °C | 8 h |
| LCO-450-1 | 450 °C | 1 h |
| LCO-450-2 | 450 °C | 2 h |
| LCO-450-4 | 450 °C | 4 h |
| LCO-450-8 | 450 °C | 8 h |
| LCO-500-1 | 500 °C | 1 h |
| LCO-500-2 | 500 °C | 2 h |
| LCO-500-4 | 500 °C | 4 h |
| LCO-500-8 | 500 °C | 8 h |
| LCO-550-1 | 550 °C | 1 h |
| LCO-550-2 | 550 °C | 2 h |
| LCO-550-4 | 550 °C | 4 h |
| LCO-550-8 | 550 °C | 8 h |
| LCO-600-1 | 600 °C | 1 h |
| LCO-600-2 | 600 °C | 2 h |
| LCO-600-4 | 600 °C | 4 h |
| LCO-600-8 | 600 °C | 8 h |

The dried samples were weighed and their X-ray diffraction (XRD, Bruker D2 Phaser) patterns were then measured. The concentrations of Li in the samples were measured using an inductively coupled plasma-optical emission spectrometer (ICP-OES, Perkin Elmer, OPTIMA7300DV).

## RESULTS AND DISCUSSION

Fig. 1 shows the XRD measurement results of the LCO-400-1, 2, 4, and 8 specimens. LCO has a hexagonal structure with cell constants of $a$=2.816 and $c$=14.08 Å consisting of the ABCABC type of vertical stacking of O-Li-O-Co-O-Li-O layers along the $c$-axis [11]. In the full scale of the $2\theta$ range shown in Fig. 1(a), significant changes were not found in the XRD patterns of the LCO specimens after the chlorination when compared to that of pristine LCO. To check for minor changes in the crystal structure, two major peaks assigned to the (003) and (104) planes were investigated, as shown in Figs. 1(b) and (c), respectively. The H-(003) peak exhibits a slight shift (<0.1°) to a lower $2\theta$ after 2 h of chlorination. Here, H-(003) represents the (003) peak in the hexagonal structure. In the LCO-400-4 and -8 specimens, new peaks are identified at around 19.2°, while their intensity levels are too low to match a phase. A down-shift is also observed in the H-(104) peak, except for LCO-400-1, which exhibits a peak position identical to that of the pristine LCO. However, the degree of the shift is subtle (<0.1°), suggesting that meaningful changes were not caused by chlorination at 400 °C based on the crystal structure.

Significant changes were observed in the XRD patterns after chlorination at 450 °C, as shown in Fig. 2. The double peaks at 65.3 and 66.3° in the LCO-450-1 and -2 specimens are replaced by a single peak at 65.8° in the LCO-450-4 and -8 specimens, suggesting that the crystal structure is changed to a higher symmetry by chlorination for 4 and 8 h. In addition, a new peak was identified at 31.5° in the LCO-450-4 and -8 specimens, as denoted by the arrows in the figure. This peak could be assigned to the (220) peak of the spinel-type $Co_3O_4$ phase (ICSD ID 24210), also shown in the figure. However, the H-(003) peak exhibits the highest intensity regard-

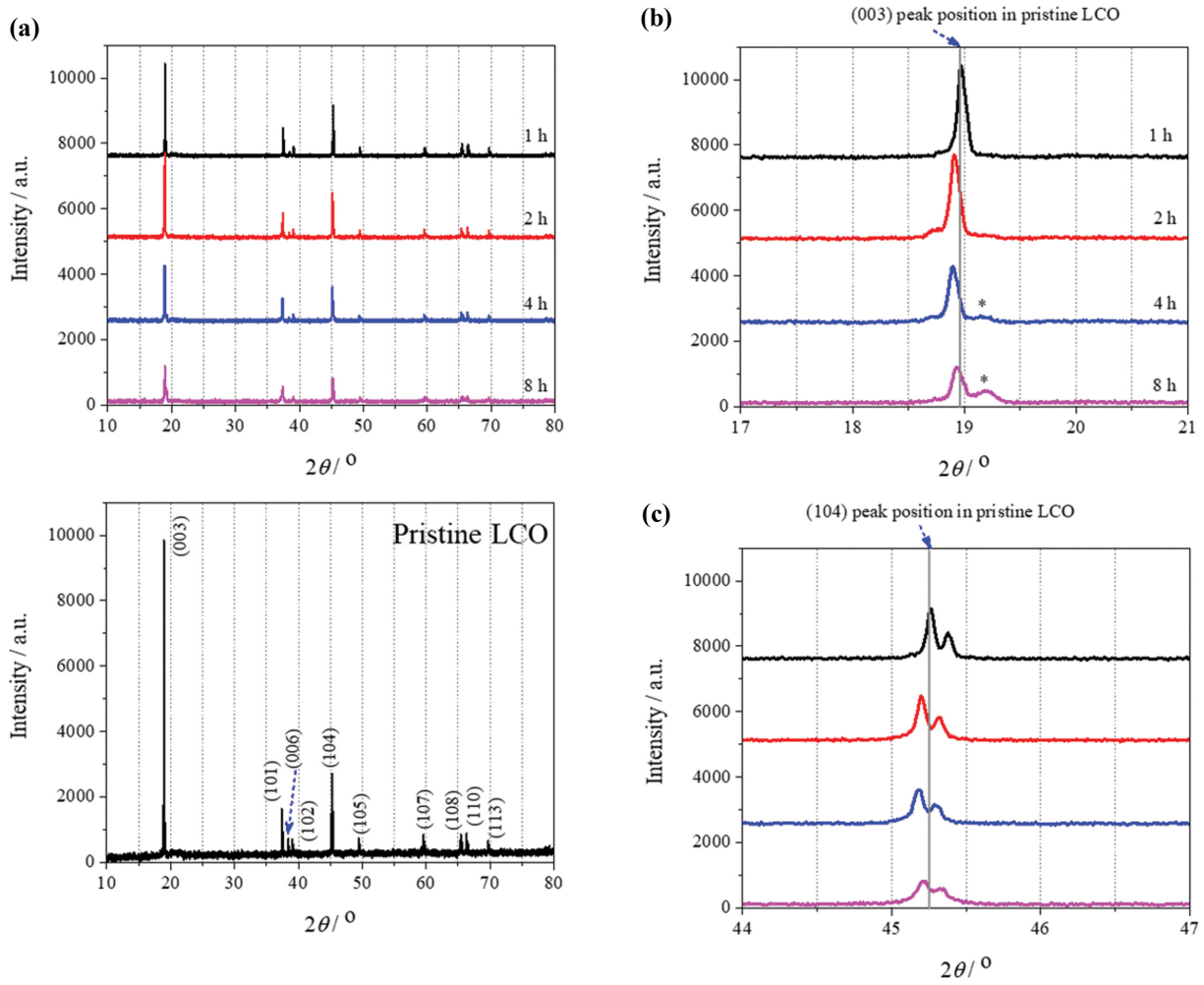


**Fig. 1. (a) XRD measurement results of LCO samples reacted with $Cl_2$ at 400 °C for 1, 2, 4, and 8 h under a 190 mL/min Ar+10 mL/min $Cl_2$ flow. The XRD measurement result of pristine LCO is also shown below. (b) Enlarged image of (a) in the $2\theta$ ranges of (b) 17-21° and (c) 44-47°.**

less of the reaction time, suggesting that the hexagonal phase is still the major chlorination product. The new peak found in the LCO-400-4 and -8 specimens at 19.2° was also observed after chlorination at 450 °C regardless of the reaction time (Fig. 2(b)). Interestingly, an increase in the reaction time resulted in an increase in the intensity of the new peak, whereas the H-(003) peak in the original position was gradually reduced in the meantime. These results suggest that the hexagonal $LiCoO_2$ phase became a Li-deficient $Li_{1-x}CoO_2$ phase after chlorination, maintaining its hexagonal structure. The shift of the H-(003) peak to a higher $2\theta$ position indicates that the new phase, $Li_{1-x}CoO_2$, has a smaller *c* parameter compared to that of the pristine LCO. On the other hand, the peak position of the H-(104) peak moved slightly to a lower $2\theta$ position in the chlorinated LCO specimens compared to that of the pristine LCO, as shown in Fig. 2(c). This result indicates that there was an increase in the *a* parameter of the $Li_{1-x}CoO_2$ phase, as a contraction in the *c* parameter was found from the H-(003) peak. The calculated lattice parameters were $a$=2.833 and $c$=13.91 Å in the LCO-450-8 specimen, while the parameters were $a$=2.816 and $c$=14.03 Å in the pristine LCO. The *c* parameter of LCO-450-8 was similar to that of $Li_{0.19}CoO_2$, while the *a* parameter was out of the range, i.e., 2.805≤a≤2.820 Å, as observed during an in-situ XRD measurement of $Li_{1-x}CoO_2$ [12,13]. Therefore, it can be theorized that chlorination resulted in a crystal structure of the $Li_{1-x}CoO_{2-y}$ phase due to liberation of oxygen instead of the $Li_{1-x}CoO_2$ phase, which was observed during the electrochemical charging-discharging experiments ($LiCoO_2 \leftrightarrow x\ Li^+ + Li_{1-x}CoO_2 + x\ e^-$). In consideration of the findings at 450 °C, the following reaction equations were derived as the chlorination mechanism:

$$LiCoO_2 + x\ Cl_2(g) \rightarrow Li_{1-x}CoO_{2-y} + x\ LiCl + y/2\ O_2(g) \quad (2)$$

$$Li_{1-x}CoO_{2-y} + (1-x)/2\ Cl_2(g) \rightarrow 1/3\ Co_3O_4 + (1-x)\ LiCl + (1/3-y/2)\ O_2(g) \quad (3)$$

The formation of the $Co_3O_4$ phase was identified even after 1 h of chlorination at 500 °C, as shown in Fig. 3(a). Note that the relative intensity between the H-(003) peak at around 19° and the H-(101) peak at around 37° changed dramatically as a function of the reaction time. We carefully examined the H-(101) peak, as shown in Fig. 3(b), where the dramatic change of the crystal structure is

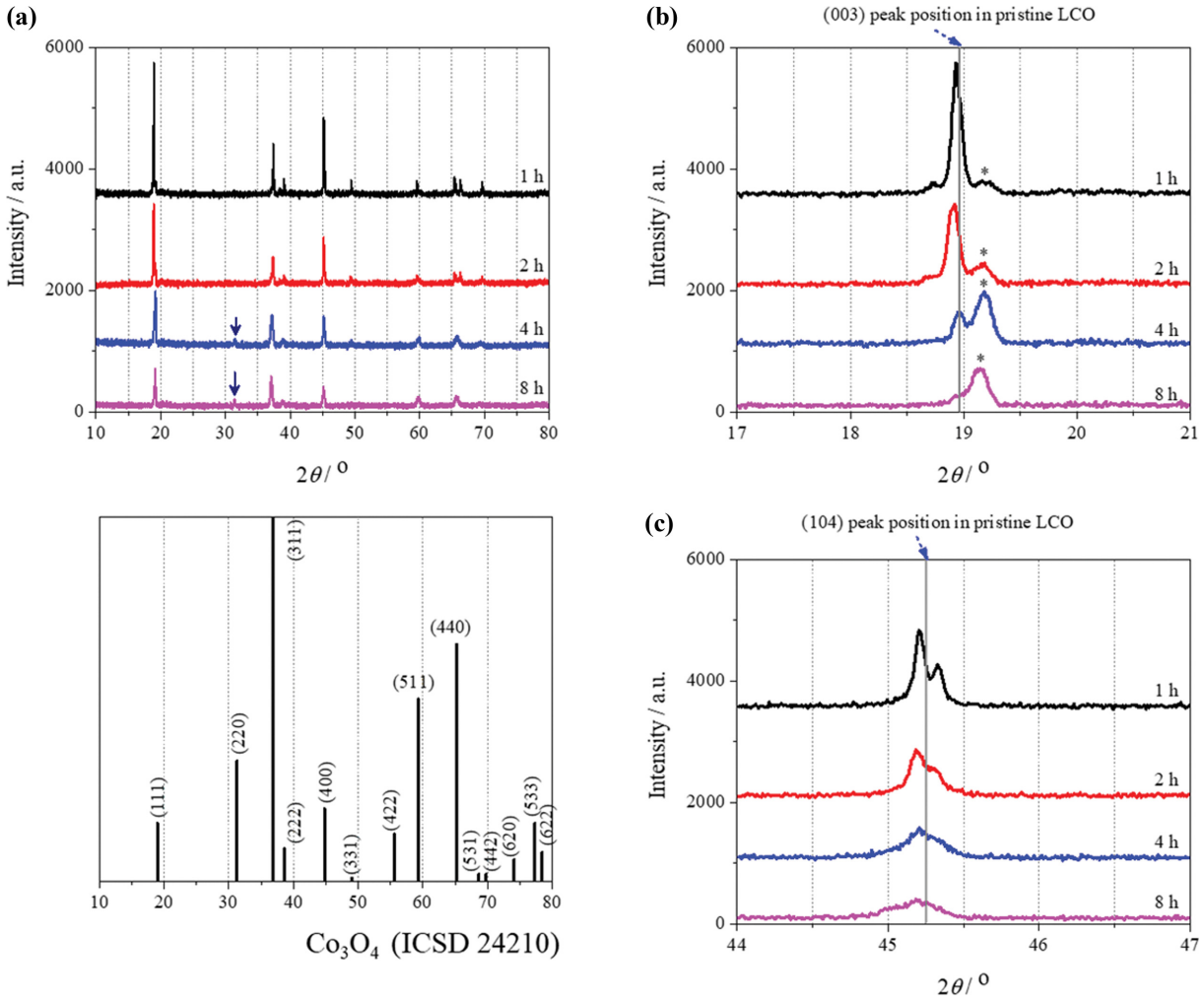


**Fig. 2. (a) XRD patterns of LCO samples reacted with $Cl_2$ at 450 °C for 1, 2, 4, and 8 h under a 190 mL/min Ar+10 mL/min $Cl_2$ flow. The XRD pattern of the $Co_3O_4$ phase (ICSD 24210) is also shown. Enlarged images of (a) in the $2\theta$ ranges of (b) 17-21° and (c) 44-47°.**

well demonstrated. The major peak of LCO-500-1 can be matched to the H-(101) peak of the pristine LCO and the broad peak at around 37.1° indicates the presence of the $Li_{1-x}CoO_{2-y}$ phase observed at 450 °C. The $Li_{1-x}CoO_{2-y}$ phase became the dominant phase in LCO-500-2 with a minor proportion of the $LiCoO_2$ phase. When the reaction time is increased to 4 h, the $LiCoO_2$ phase disappears and the peak position of the $Li_{1-x}CoO_{2-y}$ phase moves to a lower $2\theta$ position due to the presence of the $Co_3O_4$ phase. This shift continues with an increase in the reaction time to 8 h, resulting in a peak position similar to that of the S-(311) peak. Here, S-(311) represents the (311) peak in the spinel-type $Co_3O_4$ phase. This result is in good agreement with the findings at 450 °C, for which it was proposed that chlorination results in a sequential change of the crystal structure from $LiCoO_2$ to $Li_{1-x}CoO_{2-y}$ and $Co_3O_4$. Identical behavior was found in the H-(003) peak shown in Fig. 3(c). In the LCO-500-1 specimen, the major peak was found at the H-(003) peak position of the pristine LCO along with the minor peak from the $Li_{1-x}CoO_{2-y}$ phase found in LCO-450-8. The relative intensity of the $Li_{1-x}CoO_{2-y}$ phase increased compared to that of the $LiCoO_2$ phase in LCO-500-2. In LCO-500-4, the two peaks merged into a single peak in the middle of the S-(111) peak and the H-(003) peak of the $Li_{1-x}CoO_{2-y}$, phase, suggesting that these two phases contributed to this peak to a similar extent. The merged peak moved to a lower $2\theta$ position in LCO-500-8, suggesting that a relative amount of the $Co_3O_4$ phase was increased compared to the $Li_{1-x}CoO_{2-y}$ phase during the course of chlorination between 4 and 8 h. It is important to note here that the weight of the LCO-500-8 specimen was only 74% of the initial weight, though 82% is an ideal value based on complete conversion of the $LiCoO_2$ phase to the $Co_3O_4$ phase. Though the chlorination of Co oxides was not intensively studied, the chlorination of $Co_3O_4$ was observed at a temperature above 300 °C, as was the sublimation of $CoCl_2$, the reaction product, when the temperature exceeded 600 °C [14]. Accordingly, it is proposed that the chlorination of the $Co_3O_4$ phase proceeded at 500 °C via the following reaction equation:

$$Co_3O_4 + 3\,Cl_2(g) \rightarrow 3\,CoCl_2 + 2\,O_2(g) \quad (4)$$

The XRD patterns measured after chlorination at 550 °C were somewhat different from those in the abovementioned results. As shown in Fig. 4(a), the S-(220) peak at around 31° exhibits very low

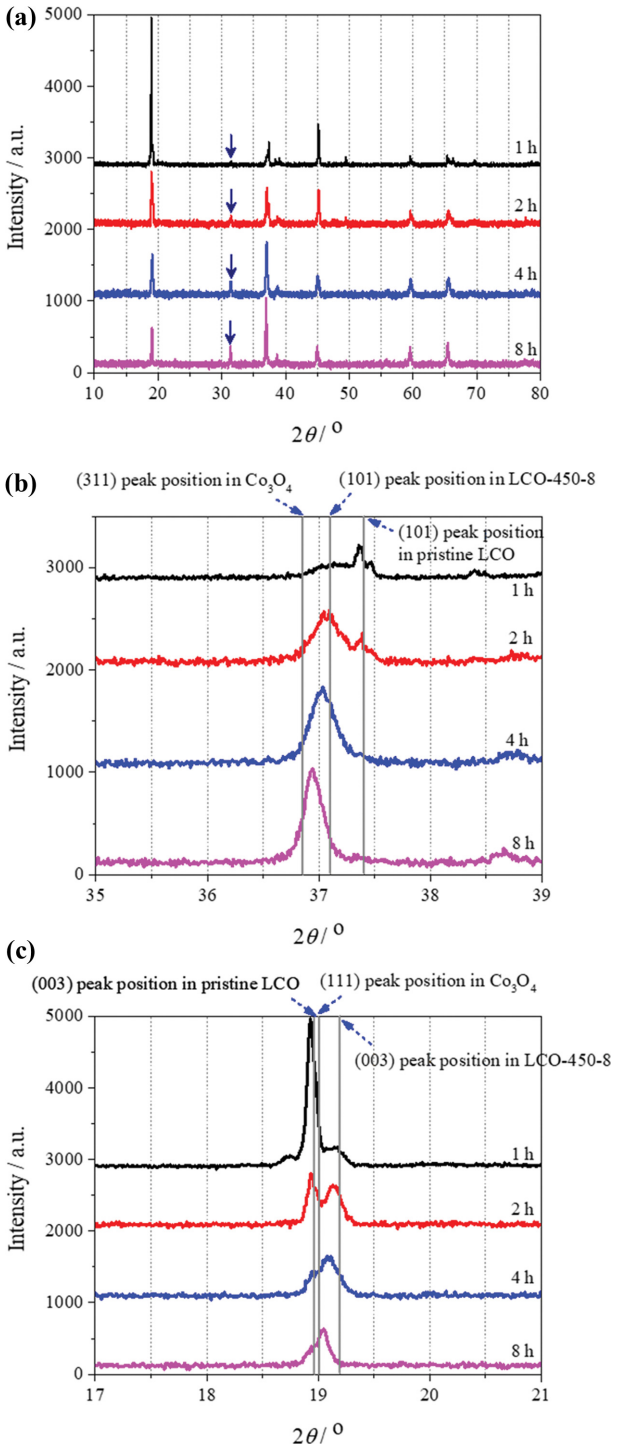


**Fig. 3. (a) XRD patterns of LCO samples reacted with $Cl_2$ at 500 °C for 1, 2, 4, and 8 h under a 190 mL/min Ar+10 mL/min $Cl_2$ flow. Enlarged images of (a) in the 2$\theta$ ranges of (b) 35-39° and (c) 17-21°.**

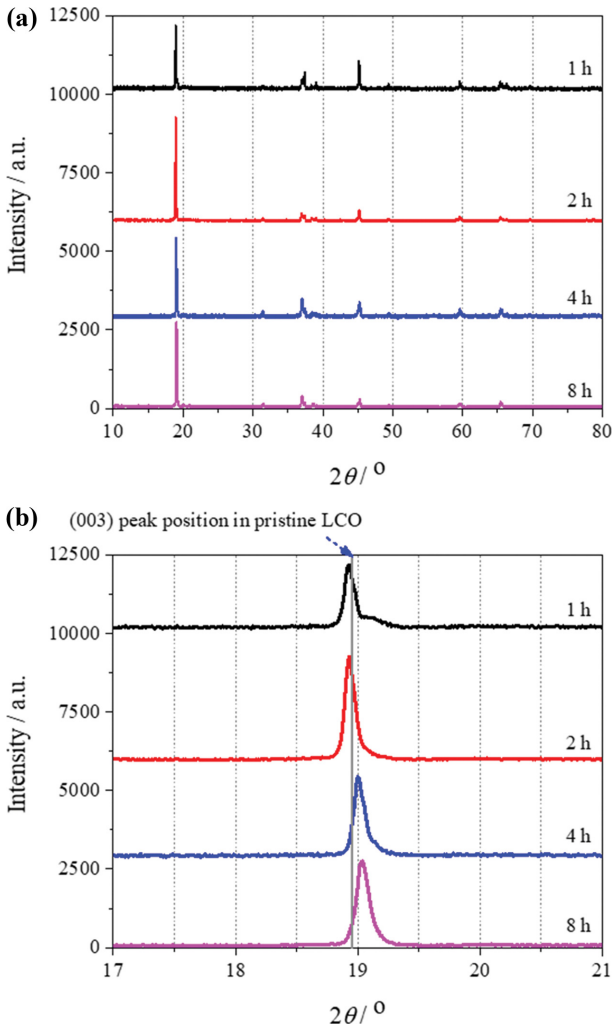


**Fig. 4. (a) XRD measurement results of LCO samples after chlorination at 550 °C for 1, 2, 4, and 8 h under a 190 mL/min Ar+ 10 mL/min $Cl_2$ flow. (b) Enlarged image of (a) in the 2$\theta$ range of 17-21°.**

intensity regardless of the reaction time. In addition, no signs of a new phase or structural transition are found in the entire range of the reaction time. It is important to note that the H-(003) peak position is in line with that of the pristine LCO without any signs of other phases, as shown in Fig. 4(b). Though the peak from the $Li_{1-x}CoO_{2-y}$ phase could be identified after chlorination at 500 °C, it was difficult to find at 550 °C. These findings can be explained by the thermal decomposition of the $Li_{1-x}CoO_{2-y}$ phase, as demonstrated earlier [15]. The thermal decomposition of $Li_{0.65}CoO_2$ and $Li_{0.81}CoO_2$ started at 250 °C, while the fully lithiated $LiCoO_2$ phase was thermally stable up to 600 °C [15]. Therefore, it is theorized that thermal decomposition occurred at 550 °C via the following reaction equation:

$$Li_{1-x}CoO_{2-y} \rightarrow (1-x)\ LiCoO_2 + x/3\ Co_3O_4 + (x/3-y/2)\ O_2(g) \quad (5)$$

In addition, the small amount of the $Co_3O_4$ phase can be explained by the chlorination of this phase, as observed at 500 °C, because the chlorination product, $CoCl_2$, is dissolved and removed from the oxide-form residue during the subsequent water washing step. Therefore, the oxide-form chlorination products at 550 °C consist mainly of the $LiCoO_2$ phase with a minor amount of the $Co_3O_4$ phase, due to simultaneous progress of the chlorination reactions (Eqs. (2)-(4)) and the thermal decomposition (Eq. (5)).

The formation of the $Co_3O_4$ phase was promoted again with an

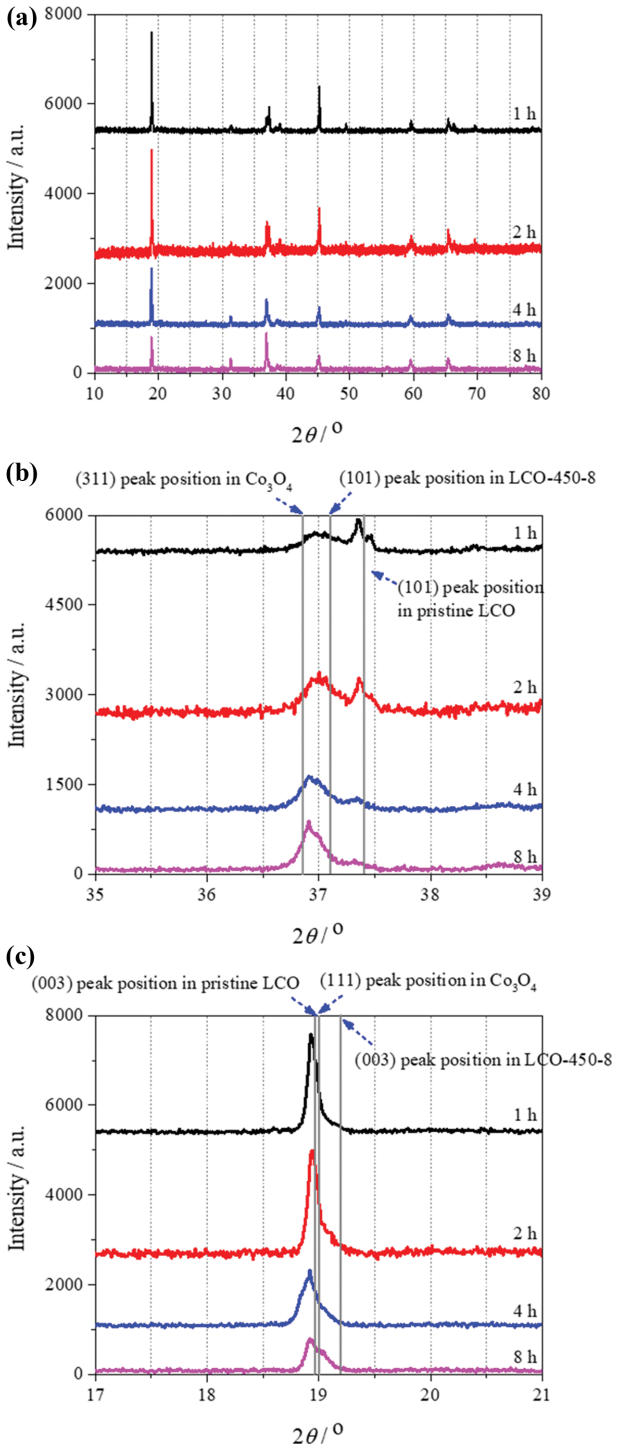


**Fig. 5. (a) XRD measurement results of LCO samples after chlorination at 600 °C for 1, 2, 4, and 8 h under a 190 mL/min Ar+ 10 mL/min $Cl_2$ flow. Enlarged images of (a) in the 2$\theta$ ranges of (B) 35-39° and (c) 17-21°.**

increase in the reaction temperature from 550 to 600 °C, as shown in Fig. 5(a). According to the relative peak intensity between the H-(003) peak and the S-(311) peak, the major chlorination product was changed from the former in LCO-600-1, -2, and -4 to the latter in LCO-600-8. The behavior of the H-(101) and S-(311) peaks was analyzed, as shown in Fig. 5(b). The presence of the $LiCoO_2$ phase was verified in the entire range of the reaction time, indicating that thermal decomposition occurred at 600 °C. A broad peak that could be assigned to both the S-(311) peak and the H-(101) peak in the $Li_{1-x}CoO_{2-y}$ phase was observed at around 37°. According to the position of this peak in LCO-600-4 and -8, it likely originated from the $Co_3O_4$ phase. Upon a closer examination of the H-(003) and S-(111) peaks, as shown in Fig. 5(c), the absence of the $Li_{1-x}CoO_{2-y}$ phase was clearly confirmed, which is in line with the findings from 550 °C. These results show that the chlorination reactions (Eqs. (2)-(4)) and the thermal decomposition (Eq. (5)) occur simultaneously at 600 °C, which was also observed at 550 °C. However, the major chlorination product of LCO-600-8 was the $Co_3O_4$ phase, while it was $LiCoO_2$ in LCO-550-8. This difference emphasizes the importance of the reaction temperature during the chlorination of LCO and may have originated from the relative increase in the reaction rate of $Li_{1-x}CoO_{2-y}$ chlorination (Eq. (3)).

The reaction mechanism for the chlorination of LCO was constructed as shown in Fig. 6 based on the XRD analysis results. Chlorination begins at 400 °C to produce the Li-deficient $Li_{1-x}CoO_{2-y}$ phase (Eq. (2)). Above 450 °C, the $Li_{1-x}CoO_{2-y}$ phase is chlorinated to produce the $Co_3O_4$ phase (Eq. (3)). In the temperature range of 500-600 °C, the chlorination of the $Co_3O_4$ phase starts to produce $CoCl_2$ (Eq. (4)). The thermal decomposition of the $Li_{1-x}CoO_{2-y}$ phase occurs along with chlorination in the range of 550-600 °C to produce the $LiCoO_2$ and $Co_3O_4$ phases (Eq. (5)). Note that a change in the reaction temperature can lead to a significantly different reaction product, because the rate of each reaction is independently affected by the reaction temperature.

The following equation was employed in conjunction with the ICP-OES results to calculate the amount of Li removed by chlorination:

$$\text{Li removal ratio} = \text{Removed amount of Li} / \text{Initial amount of Li} \quad (6)$$

The effect of the chlorination temperature on the Li removal ratio is shown in Fig. 7(a), where an increase in the reaction temperature resulted in an increase in the Li removal ratio in the temperature range of 400-500 °C. The ratio reached 0.83 after 4 h of chlorination at 500 °C. At 550 and 600 °C, the Li removal ratios were lower than that at 500 °C, as expected from the XRD results. This result suggests that the thermal decomposition played a negative role in the formation of $Co_3O_4$ (Eq. (3)) by returning a part of the $Li_{1-x}CoO_{2-y}$ phase to the $LiCoO_2$ phase. According to the findings of this work, a temperature of 500 °C is offered as the optimum condition for the chlorination of LCO. Though a high Li removal ratio was also observed at 600 °C, this temperature was not recommended due to the potential loss of Co via the sublimation of $CoCl_2$ observed at 600 °C [14]. Accordingly, the effect of the reaction time was investigated at 500 °C, as shown in Fig. 7(b). It is interesting to find that more than half of Li was removed after 1 h of chlorination. An increase in the reaction time resulted in an increase in the Li removal ratio, while the increase was relatively small between the LCO-500-4 (0.83) and LCO-500-8 (0.86) specimens. After 8 h of chlorination (LCO-500-8) 14% of Li remained; the effect of the remaining Li on the re-synthesized LCO is unclear at present. Additional investigations are necessary to link the effect of the Li removal

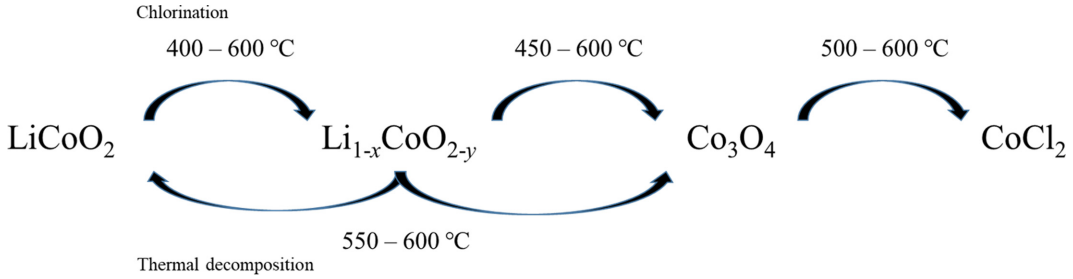


**Fig. 6. Reaction mechanism for the chlorination and thermal decomposition of $LiCoO_2$.**

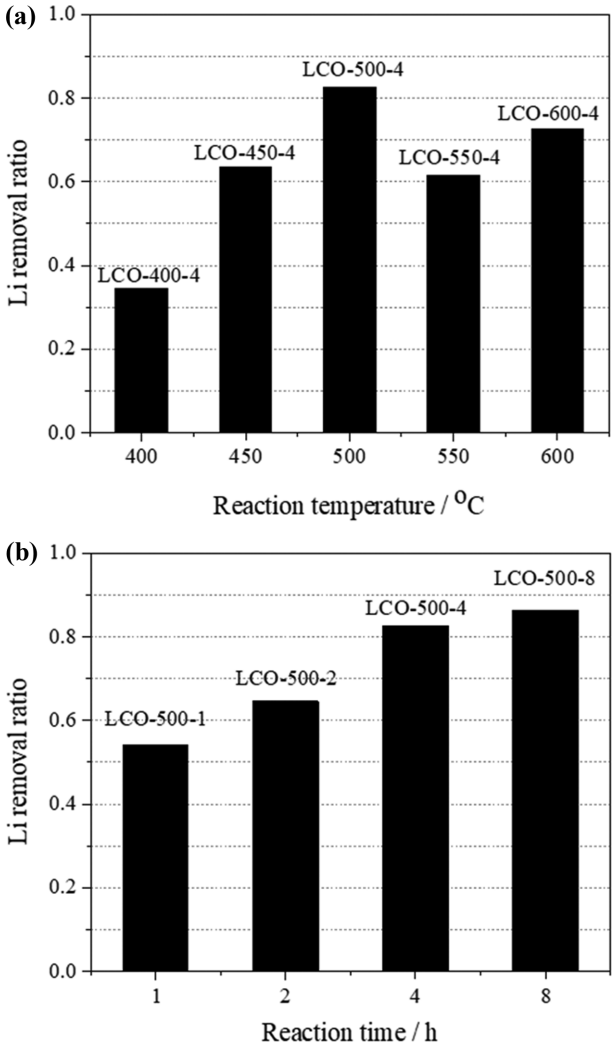


**Fig. 7. Effects of chlorination (a) the temperature and (b) the time on the Li removal ratio under a 190 mL/min Ar+10 mL/min $Cl_2$ flow. (a) Chlorination experiments were conducted for 4 h at each reaction temperature. (b) Chlorination experiments were conducted at 550 °C for each reaction time.**

ratio and the electrochemical performance of re-synthesized LCO.

Regarding the application of the chlorination technique in degraded LCO originating from used LIBs, Wang et al. [16] reported that, after electrochemical cycling, a significant fraction of LCO particles were severely strained and fractured along with defects. In addition, cation disorder in the octahedral site layers and formation of spinel oxide with Li in the tetrahedral site were observed. These findings suggest that various Li-O bonds are present in degraded LCO. Though each Li-O bond in degraded LCO may react with $Cl_2$ differently, it was shown through this work that the progress of the chlorination can be controlled by the temperature and time. Therefore, it is expected that the chlorination technique can be applied to degraded LCO after refining the operating conditions.

It is unclear at this point whether the recovered $Co_3O_4$ with a certain fraction of LCO is suitable for re-synthesis, because electrochemical performance of LCO is affected by various conditions, such as shape, particle size, and crystallinity of $Co_3O_4$ precursor. Therefore, it is required to evaluate the electrochemical performance of re-synthesized LCO, which will be the next move of our group.

## CONCLUSIONS

The key findings in this work can be summarized as follows:

1) An increase in the reaction temperature promotes the chlorination of $LiCoO_2$ to produce the Li-deficient $Li_{1-x}CoO_{2-y}$ phase in the temperature range of 400-600 °C.
2) In the temperature range of 450-600 °C, the chlorination of the $Li_{1-x}CoO_{2-y}$ phase produces the $Co_3O_4$ phase.
3) In addition to 2), the $Li_{1-x}CoO_{2-y}$ phase undergoes thermal decomposition in the temperature range of 550-600 °C to produce the $LiCoO_2$ and $Co_3O_4$ phases. This behavior results in low Li removal ratios in this temperature range.
4) The $Co_3O_4$ phase reacts with $Cl_2$ to produce $CoCl_2$ in the temperature range of 500-600 °C.
5) The optimum temperature for the chlorination of LCO was found to be 500 °C.

## ACKNOWLEDGEMENTS

This work was supported by the National Research Foundation of Korea (NRF) grant funded by the Korea Government (MSIT) (NRF-2021R1F1A1056492).

## REFERENCES

1. Global EV Outlook 2021, International Energy Agency (2021).
2. T. Or, S. W. D. Gourley, K. Kaliyappan, A. Yu and Z. Chen, *Carbon Energy*, **2**, 6 (2020).
3. G. Harper, R. Sommerville, E. Kendrick, L. Driscoll, P. Slater, R.

Stolkin, A. Walton, P. Christensen, O. Heldrich, S. Lambert, A. Abbott, K. Ryder, L. Gaines and P. Anderson, *Nature*, **575**, 75 (2019).
4. H. Bae and Y. Kim, *Mater. Adv.*, **2**, 3234 (2021).
5. P. Xu, Q. Dai, H. Gao, H. Liu, M. Zhang, M. Li, Y. Chen, K. An, Y. S. Meng, P. Liu, Y. Li, J. S. Spangenberger, L. Gaines, J. Lu and Z. Chen, *Joule*, **4**, 1 (2020).
6. H. Yang, B. Deng, X. Jing, W. Li and D. Wang, *Waste Manage.*, **129**, 85 (2021).
7. X. Qu, H. Xie, X. Chen, Y. Tang, B. Zhang, P. Xing and H. Yin, *ACS Sustainable Chem. Eng.*, **8**, 6524 (2020).
8. M. K. Jeon, S.-W. Kim, H.-C. Eun, K.-Y. Lee, H. Kim and M. Oh, *Korean J. Chem. Eng.*, In press (2022) (https://doi.org/10.1007/s11814-022-1083-6).
9. D. R. Lide, ed., *CRC handbook of chemistry and physics*, Internet Version 2006, Taylor and Francis, Boca Raton, FL (2006).
10. J. B. Goodenough, K. Mizushima and P. J. Wiseman, Eur. Patent, EP0017400A1 (1979).
11. K. Mizushima, P. C. Jones, P. J. Wiseman and J. B. Goodenough, *Mater. Res. Bull.*, **15**, 783 (1980).
12. G. G. Amatucci, J. M. Tarascon and L. C. Klein, *J. Electrochem. Soc.*, **143**, 1114 (1996).
13. J. N. Reimers and J. R. Dahn, *J. Electrochem. Soc.*, **139**, 2091 (1992).
14. T. A. Anufrieva and L. E. Derlyukova, *Russ. J. Inorg. Chem.*, **52**, 1840 (2007).
15. Y. Furushima, C. Yanagisawa, T. Nakagawa, Y. Aoki and N. Muraki, *J. Power Sources*, **196**, 2260 (2011).
16. H. Wang, Y.-I. Jang, B. Huang, D. R. Sadoway and Y.-M. Chiang, *J. Electrochem. Soc.*, **146**, 473 (1999).